



Ab initio study of oxygen segregation in silicon grain boundaries: The role of strain and vacancies

Rita Maji^a, Eleonora Luppi^{b,*}, Nathalie Capron^c, Elena Degoli^{d,e,f,*}

^a Dipartimento di Scienze e Metodi dell'Ingegneria, Università di Modena e Reggio Emilia, Via Amendola 2 Padiglione Tamburini, I-42122 Reggio Emilia, Italy

^b Laboratoire de Chimie Théorique, Sorbonne Université and CNRS, F-75005 Paris, France

^c Sorbonne Université, CNRS, Laboratoire de Chimie Physique Matière et Rayonnement, UMR 7614, F-75005 Paris, France

^d Dipartimento di Scienze e Metodi dell'Ingegneria, Università di Modena e Reggio Emilia, Via Amendola 2 Padiglione Morselli, I-42122 Reggio Emilia, Italy

^e Centro Interdipartimentale En&Tech, Via Amendola 2 Padiglione Morselli, I-42122 Reggio Emilia, Italy

^f Centro S3, Istituto Nanoscienze-Consiglio Nazionale delle Ricerche (CNR-NANO), Via Campi 213/A, 41125 Modena, Italy



ARTICLE INFO

Article history:

Received 24 June 2020

Revised 26 September 2020

Accepted 8 November 2020

Available online 19 November 2020

Keywords:

Silicon grain boundaries

Oxygen segregation

Strain

Silicon vacancies

First principles calculations

ABSTRACT

Multi-crystalline silicon is widely used for producing low-cost and high-efficiency solar cells. During crystal growth and device fabrication, silicon solar cells contain grain boundaries (GBs) which are preferential segregation sites for atomic impurities such as oxygen atoms. GBs can induce charge carriers recombination significantly reducing carrier lifetimes and therefore they can be detrimental for Si device performance. We studied the correlation between structural, energetic and electronic properties of $\Sigma 3\{111\}$ Si GB in the presence of vacancies, strain and multiple O segregation. The study of the structural and energetic properties of GBs in the presence of strain and vacancies gives an accurate description of the complex mechanisms that control the segregation of oxygen atoms. We analysed tensile and compressive strain and we obtained that local tensile strain around O impurities is very effective for segregation. We also studied the role of multiple O impurities in the presence of Si vacancies finding that the segregation is favorite for those structures which have restored tetrahedral covalent bonds. The presence of vacancies attract atomic impurities in order to restore the electronic stability: the interstitial impurity becomes substitutional. This analysis was the starting point to correlate the change of the electronic properties in $\Sigma 3\{111\}$ Si GBs with O impurities in the presence of strain and vacancies. For each structure we analysed the density of states and its projection on atoms and states, the band gaps, the segregation energy and their correlation in order to characterise the nature of new energy levels. Actually, knowing the origin of defined electronic states would allow the optimization of materials in order to reduce non radiative electron-hole recombination avoiding charge and energy losses and therefore improving solar cell efficiency.

© 2020 Acta Materialia Inc. Published by Elsevier Ltd. All rights reserved.

1. Introduction

Multi-crystalline silicon is widely used for producing low-cost and high-efficiency solar cells [1–4]. During crystal growth and device fabrication, Si solar cells contain grain boundaries (GBs) which can be detrimental for the device performance [5–7]. GBs can create deep-energy states which induce charge carriers recombination generating a reverse flux of electrons across the junction that separates the electron- and hole-conducting media. The effect is a significant reduction of carrier lifetimes [8–11]. Avoiding the recombination is extremely important for an optimisation of solar cells

efficiency. This can be achieved by tuning the energy levels in the materials.

A novel view about Si GBs was given by Raghunathan et al. [12] whom predicted that GBs could instead be beneficial to solar energy conversion. They proposed to exploit the electronic properties of GBs in order to design novel and efficient solar cells. However, electronic properties of GBs can be very difficult to tune. In fact, GB structures are very variegated and can easily form vacancies with deep defect electronic states, accelerating charge dissipation [13]. Besides, GBs are also preferential segregation sites for various impurity species which can significantly influence the electrical properties [14–18]. Segregation activity can create recombination centers and have a substantial detrimental impact on the conversion efficiency of solar cells [19,20].

* Corresponding authors.

E-mail addresses: eleonora.luppi@upmc.fr (E. Luppi), elena.degoli@unimore.it (E. Degoli).

Oxygen atoms are inevitably introduced during solar-cell crystal growth which usually form precipitate recombination centers with different morphology [21,22]. Complex mechanisms control the segregation of oxygen atoms at Si GBs which is influenced by the size and the orientation of the grains and also by the presence of vacancies and strain in the GBs [17,19,22–28]. Therefore, the possibility or not to engineer GBs for photovoltaics applications, and more generally to improve solar cell efficiency, depends also on their capacity to segregate different types of impurities such as oxygen atoms.

Understanding the correlation between structural and electronic properties of GBs in the presence of vacancies and interacting atomic impurities is crucial to improve solar cells technology.

In this work we studied from first-principles how the electronic properties of $\Sigma 3\{111\}$ Si GB, in the presence of strain and vacancies, are modified by multiple oxygen segregation. We have chosen the $\Sigma 3\{111\}$ GB because it is the most likely to form in Si solar cell [17,29,30]. This is also the most stable GB since there are no dangling bonds and little bond distortion [31]. Its electrical activity and gettering ability is negligible [16,31]. However, the behaviour of $\Sigma 3\{111\}$ Si GB drastically changes in the presence of strain and vacancies [23,31]. In fact, these dislocations cause lattice distortion around sites which can act as gettering center for impurity.

Starting from the unstrained $\Sigma 3\{111\}$ Si GB, we considered tensile and compressive strain differently applied to the GB. Then, multiple oxygen atoms were introduced in the strained GBs (SGB) in many different possible configurations. For each configuration and type of strain, we calculated the oxygen segregation energy revealing the factors influencing the segregation. The same methodology was then implemented to investigate the oxygen segregation in $\Sigma 3\{111\}$ Si GB with a Si vacancy (VGB). Starting from $\Sigma 3\{111\}$ GB with a Si vacancy, we considered multiple oxygen atoms in different structural configurations within the GB, and also in this case we studied the mechanisms that regulate the oxygen segregation.

The electronic properties for each structure have been investigated by analysing the density of states (DOS) and the band gaps versus the segregation energy. We characterised the origin of the new energy levels due to the presence of GBs, strain, vacancies and/or oxygen atoms. Actually, knowing the origin of the electronic states permits to find strategies to reduce non radiative electron-hole recombination avoiding charge and energy losses and therefore improving solar cell efficiency.

2. Methodology and grain boundary structure

The $\Sigma 3\{111\}$ Si GB consists of two grains of Si forming an interface along the crystallographic plane $\{111\}$ (coincidence site lattice). The two Si grains are misoriented with respect to one another by an angle $\Omega = 60^\circ$. In Fig. 1 we show the $\Sigma 3\{111\}$ orthorhombic supercell ($a \neq b \neq c$ and $\alpha = \beta = \gamma = 90^\circ$) composed of 96 Si atoms generated with *GB Studio* program [32]. The lattice parameters are $a=13.30$ Å, $b=7.68$ Å and $c=18.81$ Å. It is possible to observe the presence of two GBs, one in the middle of the cell and the other at the edges of the cell due to the periodic boundary conditions.

Then, we inserted O atoms in the $\Sigma 3\{111\}$ Si GB which was additionally strained (see section: 3.1) and in which we also created a vacancy (see section: 3.2). For each structure we calculated the impurity and the segregation energy of oxygen atoms. Moreover, in order to compare all the structures, we took Si bulk as a reference. In this case, we used a cubic supercell ($a = b = c$ and $\alpha = \beta = \gamma = 90^\circ$) of 64 atoms with $a=10.86$ Å. This value for a was obtained by the experimental lattice constant 5.431 Å for a face-centered cubic unit cell of two Si atoms [33]. We also report the calculated Si bulk modulus $B = 95.4$ GPa and the elastic tensor components $c_{11} = 159.8$ GPa and $c_{12} = 63.2$ GPa. These values are

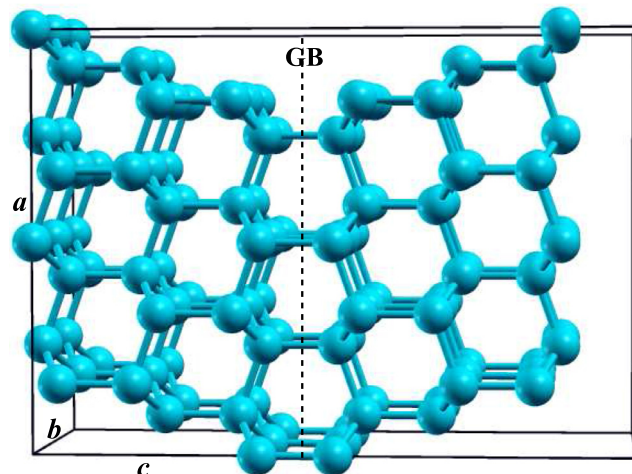


Fig. 1. $\Sigma 3\{111\}$ Si GB orthorhombic supercell: a , b and c are the lattice parameters. The dotted line shows the GB between two Si grains.

in good agreement with other theoretical calculations and with the experimental values $B = 99.2$ GPa, $c_{11} = 167.5$ GPa and $c_{12} = 65.0$ GPa [33].

The calculations were performed using density functional theory (DFT) as implemented in the plane-wave based Vienna Ab initio Simulation Package (VASP) [34,35]. We employed the generalised gradient approximation PBE for the exchange-correlation functional [36] and projector augmented-wave (PAW) pseudopotentials with a cutoff of 400 eV. K-points sampling within the Monkhorst Pack scheme [37] was used for integration of Brillouin-zone together with the linear tetrahedron method including Blöchl corrections [38]. In particular, we used a k-mesh of $3 \times 3 \times 3$ to calculate energy properties of the structures and a k-mesh of $7 \times 7 \times 7$ to calculate their density of states (DOS). For the structural optimisation, we used as threshold on the forces the value of 10^{-2} eV/Å per atom.

The choice of the PBE functional was motivated by the need to find a balance between accuracy and computational cost. In the recent years, new GGA functionals for solids have been proposed to improve the description of structural properties [39]. However, the improvements over PBE are not systematic [39] and in some cases even less accurate [40].

Concerning the electronic properties, it is well known that PBE underestimates the electronic band gaps. For Si bulk we obtain 0.574 eV compared with the experimental value of 1.25 eV. [41]. Hybrids functionals or GW corrections can be used to obtain higher accuracy, but the computational cost is very high for the systems studied here. However, despite the underestimation of the absolute values of the gaps, we believe that the trend of the electronic properties is also valid in PBE. For example, for Si bulk the effect of an hybrid functional or GW corrections is to rigidly shift the band structure [42,43].

3. Results and discussion

3.1. Oxygen atoms in $\Sigma 3\{111\}$ Si GB : the role of strain

The formation energy of $\Sigma 3\{111\}$ Si GB is calculated as

$$E_{\text{GB}}^{\text{f}} = \frac{E_{\text{GB}} - n_{\text{GB}}e_{\text{B}}}{2A}, \quad (1)$$

where E_{GB} is the energy of the GB, n_{GB} is the number of atoms (96) in the GB supercell, e_{B} is the energy per Si atom taken from the Si cubic crystal structure, A is the GB cross-section area and

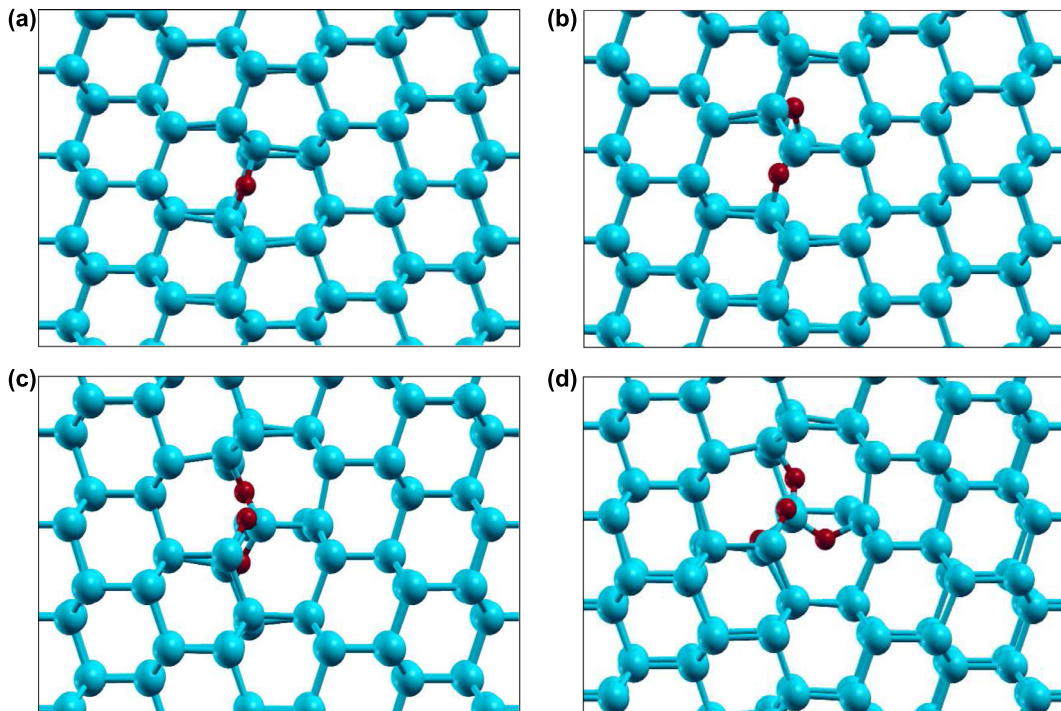


Fig. 2. $\Sigma 3\{111\}$ Si GB structures with a number $n = 1$ (a), 2 (b), 3 (c) and 4 (d) of O atoms (red balls) in interstitial configurations. Between all the different structures investigated, here we show those that have the lowest total energy (LE).

the scaling factor 1/2 denotes the presence of two GBs in the supercell [15]. We obtained a very low formation energy $E_{GB}^f = 0.002$ eV/ \AA^2 ($E_{GB}^f = 0.05$ J/m²) which is the indication of the very regular structure of the $\Sigma 3\{111\}$ GB, i.e. bond lengths and angles are close to the Si bulk [14,15].

We started by inserting O atoms in the $\Sigma 3\{111\}$ Si GB in different configurations and we optimised the structures. In the Supp. Mat. we show examples of structures before and after optimisation. We always obtain that the O atoms segregate at bond-centered position between two Si atoms. Therefore, the optimised structures have no coordination defects as all Si atoms restored their tetrahedral coordination (see Fig. 2) [23]. Moreover, the position of the O atoms in the GB can change of sites between the different structures, but the structural parameters (bond lengths and angles) and total energies differ only about 0.01 %.

To investigate the interaction between the O atoms and the $\Sigma 3\{111\}$ Si GB we calculated the segregation energy of the O atoms as

$$\Delta_{nOB}^{nOGB} = E^{nOGB} - E^{nOB}, \quad (2)$$

where E^{nOGB} and E^{nOB} are the impurity energies of the O atoms respectively in the GB and in the bulk Si which are calculated as

$$E^{nOGB} = E_{nO+GB} - E_{GB} - n\mu_0, \quad (3)$$

$$E^{nOB} = E_{nO+B} - E_B - n\mu_0. \quad (4)$$

E_{nO+GB} is the total energy of the GB containing n number of O atoms, E_{GB} is the total energy of the GB, μ_0 is the chemical potential of oxygen calculated as the energy per atom of an O_2 molecule in vacuum, E_{nO+B} is the total energy of the Si bulk containing n number of O atoms [44] and E_B is the total energy of Si bulk.

In Fig. 3 we show the O segregation energies for all the investigated structures which were ordered by their pressure $P_B^{nO+GB} = P_{nO+GB} - P_B$, calculated as the difference between the pressure of the GB containing n number of O atoms (P_{nO+GB}) and the pressure of the Si bulk ($P_B = 1.973$ GPa).

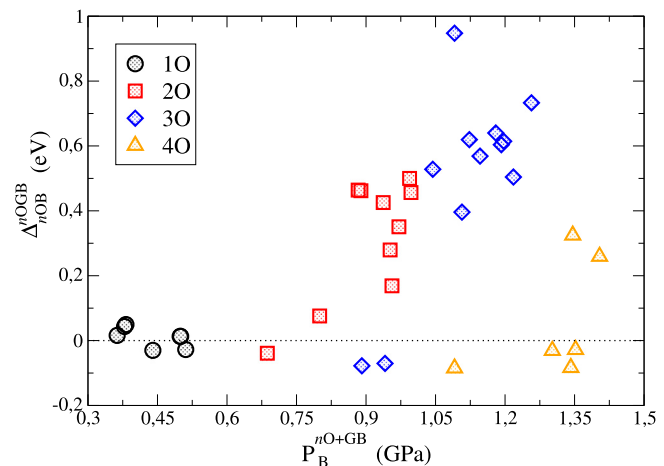


Fig. 3. O segregation energy Δ_{nOB}^{nOGB} in GB as a function of P_B^{nO+GB} . The number of O atoms is $n = 1, 2, 3$ and 4.

Most of the structures have positive segregation energies (not larger than 1 eV) while few structures have negative segregation energy (not lower than -0.1 eV). In Table 1 we explicitly report the O segregation energies for n equal to 1, 2, 3 and 4 interstitial O atoms but only for those structures that have the highest and the lowest total energy (E_{nO+GB}). In the Supp. Mat. we reported the values for all the structures presented in Fig. 3.

The behaviour we obtained for Δ_{nOB}^{nOGB} shows that oxygen atoms prefer not to segregate at GB as the structures become energetically unfavourable. Therefore, this result confirms that $\Sigma 3\{111\}$ Si GB has no gettering ability to solute oxygen atoms [16,45]. These structures present very similar energetic properties due to their similar structural properties: this fact impacts also the electronic properties. In Fig. 4 we show the DOS for the $\Sigma 3\{111\}$ Si GB without oxygen atoms (GB) and for $\Sigma 3\{111\}$ Si GBs with multiple oxy-

Table 1

Oxygen segregation energy Δ_{nOB}^{nOGB} (eV) and P_B^{nO+GB} (GPa) for n equal to 1,2,3 and 4 oxygen atoms. The values are reported for the LE (lowest total energy) and HE (highest total energy) GB.

	P_B^{1O+GB}	Δ_{1OB}^{1OGB}	P_B^{2O+GB}	Δ_{2OB}^{2OGB}	P_B^{3O+GB}	Δ_{3OB}^{3OGB}	P_B^{4O+GB}	Δ_{4OB}^{4OGB}
HE	0.382	0.049	0.994	0.499	1.091	0.947	1.346	0.325
LE	0.440	-0.030	0.687	-0.039	0.891	-0.078	1.091	-0.085

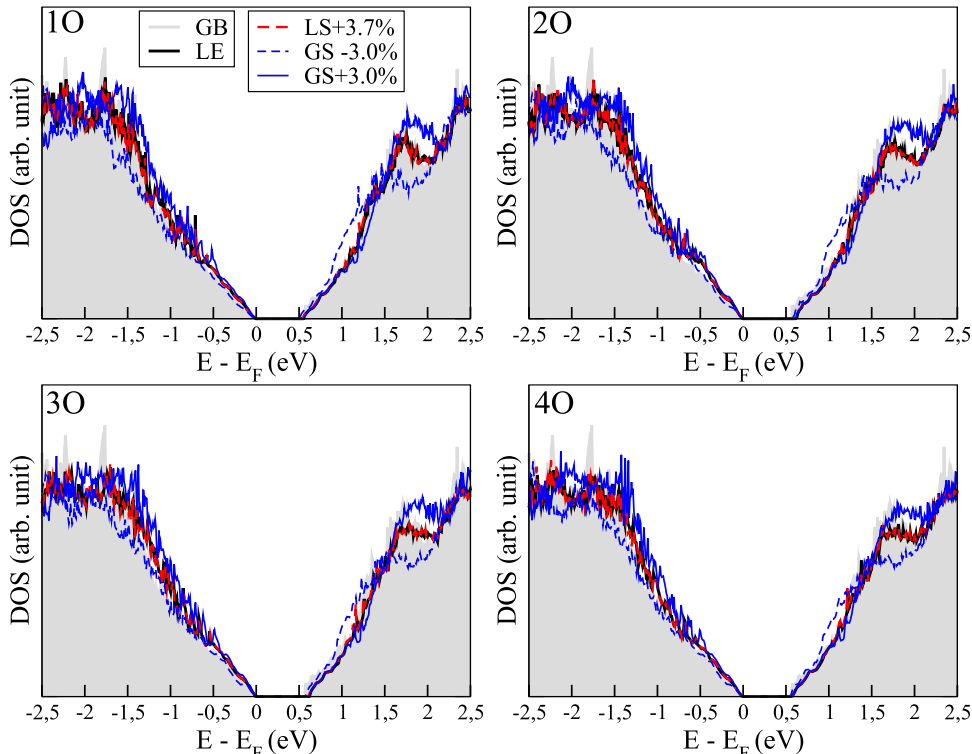


Fig. 4. Density of states of the GB (grey shadow), LE (black) and SGB with local strain (red) and global strain (blue) structures. The number of O atoms is $n = 1, 2, 3$ and 4. The percentage of strain is reported in the legend and corresponds to the bond length deformation in the case of local strain and to the lattice parameter deformation in the case of global strain.

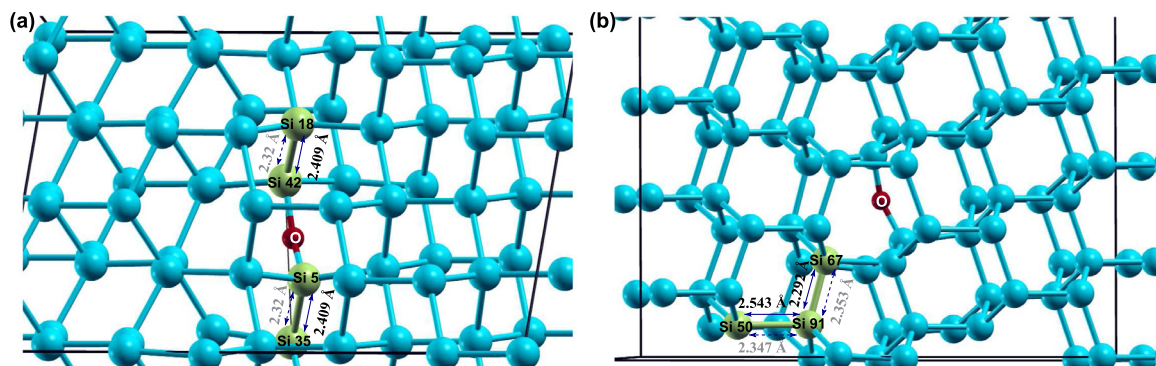


Fig. 5. $\Sigma 3\{111\}$ Si GB with one O atom (red ball) under local strain. (a) two bonds close to the O atom are elongated by +3.7%. (b) two bonds far from the O atom are modified of about -2.6% and +8.3%. Modified bond lengths are reported in black (strained) and grey (unstrained).

gen atoms and lowest total energy (LE). The DOS are almost superimposable. The comparison with the structures with the highest total energy (HE) is reported in the Supp. Mat. showing the same behaviour.

The energetically unfavourable segregation of oxygen atoms at $\Sigma 3\{111\}$ Si GB can change in the presence of strain. In fact, a correlation has been found between the segregation of O atoms and strain [17,23]. O atoms seem to prefer to segregate under tensile strain. Here we show in detail the ability of strain to segregate oxygen atoms at GB.

Starting from the unstrained LE $\Sigma 3\{111\}$ Si GBs previously obtained in the presence of O atoms ($n = 1, 2, 3$ and 4), we generated two new groups of structures where the strain is simulated in this way:

- 1) Local Strain (LS) [46]: we modified some bond lengths in the LE $\Sigma 3\{111\}$ Si GB creating locally tensile/compressive strain. In Fig. 5 we show two examples for one O atom. On the left, we elongated the two Si bonds close to the O atom of 3.7% with respect to the unstrained LE structure. The strained structure is labelled

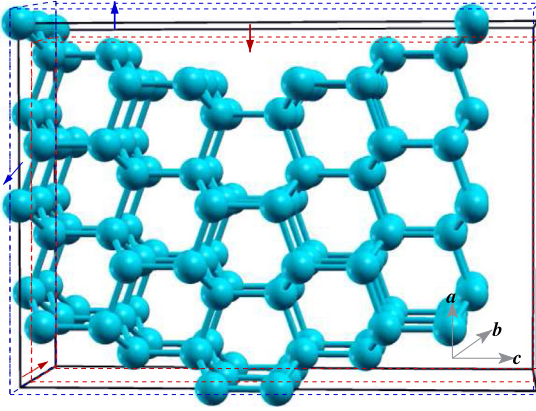


Fig. 6. $\Sigma 3\{111\}$ Si GB under global strain. The cell in black-solid line is the unstrained one, while red-dotted line and blue-dotted line represent the compressed and tensile strained cells respectively. The lattice parameter c , in the z direction, is left unchanged, while a and b , in the xy plane, are modified.

LS_{+3.7%}. On the right, instead we changed two bonds far from the O atom of about -2.6% (compression) and 8.3% (elongation). This structure is labelled LS_{-2.6%}^{+8.3%}.

- 2) Global Strain (GS): we changed the lattice parameters of the LE $\Sigma 3\{111\}$ Si GB in the x and y directions leaving the z direction unchanged. As the elongation or compression is rigidly applied to the whole structure, the bond lengths are elongated or compressed of about the same amount. Examples are shown in Fig. 6 where an elongation of +2.0% (left) and a compression of -2.0% (right) were applied to the a and b lattice parameters of the LE structure. These structures are labelled respectively GS_{+2.0%} and GS_{-2.0%} and the bond lengths are respectively elongated by about +2.0% and compressed by about -2.0%.

Applying LS and GS methodologies to the LE $\Sigma 3\{111\}$ Si GB, we realised a series of strained structures which differs by the percentage of strain and for which we calculated the segregation energy of the O atoms as :

$$\Delta_{nOGB}^{nOSGB} = E^{nOSGB} - E^{nOGB}, \quad (5)$$

where E^{nOSGB} is the impurity energy of the O atoms in the strained GB calculated as :

$$E^{nOSGB} = E_{nO+SGB} - E_{SGB} - n\mu_O, \quad (6)$$

and E^{nOGB} is defined in Eq. (3). In particular, E_{nO+SGB} is the energy of the strained GB containing n number of O atoms and E_{SGB} is the energy of the strained GB.

To keep the effect of the strain during the simulation, it is important not to fully relax the strained structures, otherwise the systems would relax to their unstrained counterpart [46]. Therefore considering first the strained GB with only one O atom we tried two different strategies to calculate the strained total energies: 1) performing a self-consistent calculation, 2) optimising the structure by constraining the Si atoms around the O atom. The results obtained for Δ_{1OGB}^{1OSGB} with the two strategies are reported in the Supp. Mat. and differ by about 3×10^{-3} eV which is also two orders of magnitude smaller than the DFT accuracy. For these reasons, for $n = 2, 3$ and 4 O atoms, we proceeded by just performing a self-consistent calculation.

In Fig. 7 we show the O segregation energies (Δ_{nOGB}^{nOSGB}) in LS GBs as a function of their pressure $P_B^{nO+SGB} = P_{nO+SGB} - P_B$, calculated as the difference between the pressure of the SGB with n number of O atoms (P_{nO+SGB}) and the pressure of the Si bulk (P_B). We found that even if locally we have a tensile strain close to the O atom, the P_{nO+SGB} , which average over the whole cell, is always positive, indicating therefore a compressive strain [46]. It is

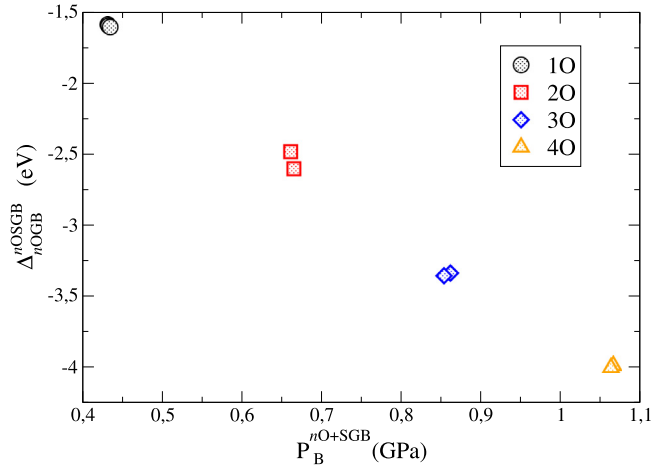


Fig. 7. Oxygen segregation energy Δ_{nOGB}^{nOSGB} in locally strained GB as a function of P_B^{nO+SGB} . The number of O atoms is $n = 1, 2, 3$ and 4 .

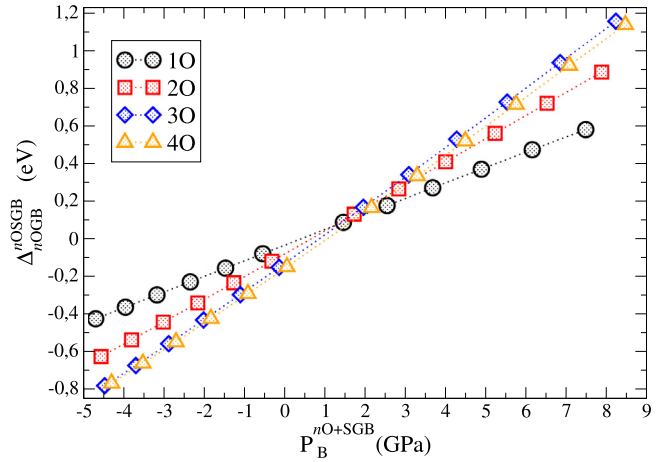


Fig. 8. Oxygen segregation energy Δ_{nOGB}^{nOSGB} in globally strained GB as a function of P_B^{nO+SGB} . The number of O atoms is $n = 1, 2, 3$ and 4 .

important to underline this point because we obtain that all the structures have negative Δ_{nOGB}^{nOSGB} which means that O segregation is expected. However, the segregation is strongly related to the local tensile strain around the O atoms. The local geometry of the boundary site where the O is segregated seems to be clearly correlated to the capacity of the GB to act as a gettering site. Moreover, the higher is the number of oxygen atoms in the strained region, the more effective is the segregation. The explicit values of Δ_{nOGB}^{nOSGB} in the case of LS are reported in Table 2 and in the Supp. Mat. for comparison with GS structures.

We point out that the values of LS considered here are only those where the strain is applied close to the O atoms. In fact, calculating the effects of strain far from the O atoms we observed that it is much less effective in fostering the segregation process. To obtain segregation energies of the same order of magnitudes as those in Table 2 we need to apply much stronger strain. For example for LS_{+8.3%} we obtain $\Delta_{1OGB}^{1OSGB} = -1.552$ eV with $P_B^{nO+SGB} = 0.466$ GPa.

In Fig. 8 we show Δ_{nOGB}^{nOSGB} in GS GBs as a function of the pressure P_B^{nO+SGB} . The trend we observe is independent on the number of O atoms. The more the pressure is negative (tensile), the more the O atoms are segregated. Instead, exactly the opposite is obtained in the case of compression. These effects seem to be progressively more pronounced as the number of oxygen atoms increases and it seems to stabilise for 3 and 4 O atoms. This behaviour, including the reversal in the oxygen segregation capacity

Table 2

Oxygen segregation energy $\Delta_{n\text{OGB}}^{\text{nOSGB}}$ (eV) in locally and globally strained GBs and $P_B^{n\text{O+SGB}}$ (GPa) for n equal to 1,2,3 and 4 oxygen atoms.

	$P_B^{1\text{O+SGB}}$	$\Delta_{1\text{OGB}}^{\text{1OSGB}}$	$P_B^{2\text{O+SGB}}$	$\Delta_{2\text{OGB}}^{\text{2OSGB}}$	$P_B^{3\text{O+SGB}}$	$\Delta_{3\text{OGB}}^{\text{3OSGB}}$	$P_B^{4\text{O+SGB}}$	$\Delta_{4\text{OGB}}^{\text{4OSGB}}$
LS _{+3.7%}	0.432	-1.589	0.665	-2.602	0.861	-3.334	1.065	-3.984
LS _{+5.7%}	0.435	-1.607	0.661	-2.482	0.853	-3.353	1.062	-3.999
GS _{+3.0%}	-4.676	-0.426	-4.543	-0.626	-4.452	-0.781	-4.282	-0.768
GS _{-0.5%}	-0.533	-0.080	-0.308	-0.120	-0.126	-0.153	-0.067	-0.150
GS _{-0.5%}	1.467	0.086	1.735	0.129	1.962	0.166	2.163	0.163
GS _{-3.0%}	7.476	0.579	7.870	0.884	8.223	1.154	8.458	1.135

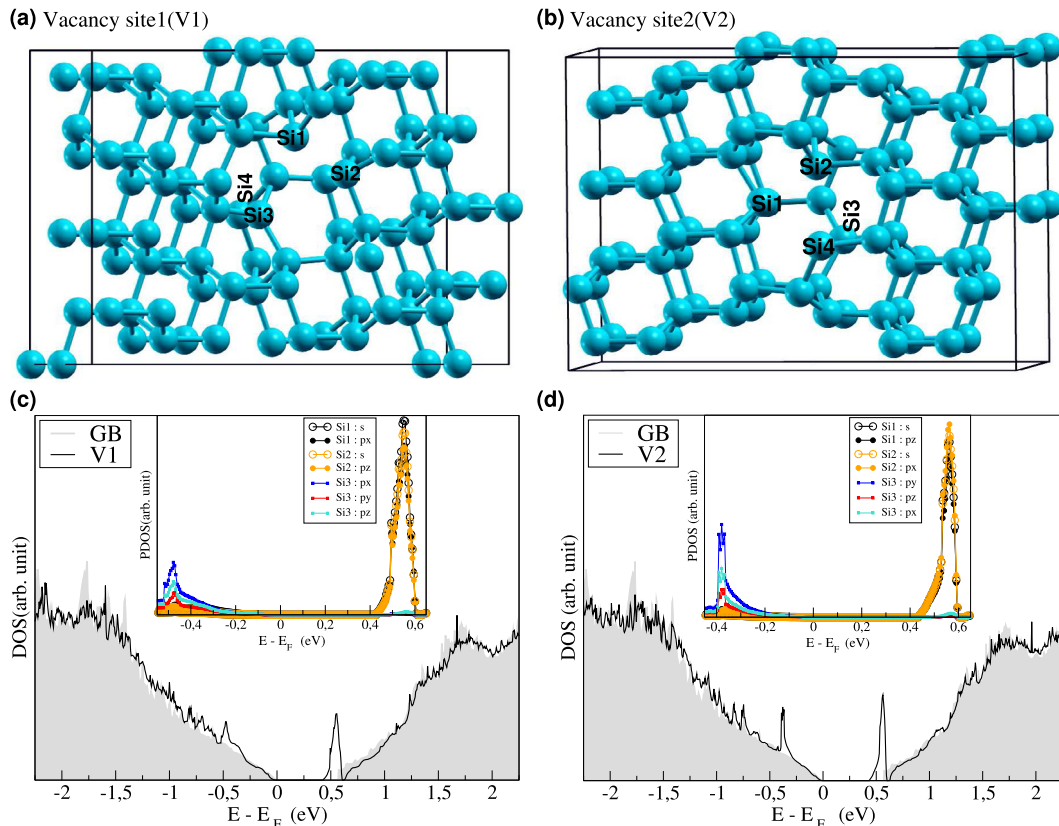


Fig. 9. Relaxed $\Sigma 3\{111\}$ Si GB with silicon vacancies labelled as V1 (a) and V2 (b). All Si atoms are four-fold coordinated except the atoms we labelled as Si1 and Si2 which are three-fold coordinated. On the bottom the DOS of the corresponding above structures ((c) V1, (d) V2) are reported with a focus in the insets that shows the projected DOS (P-DOS) of Si1, Si2 and Si3 atoms (P-DOS of atom Si4 is not reported because it is superimposable to that of atom Si3).

between tensile and compressive strain, is probably due to the fact that under tensile strain silicon and oxygen atoms can mimick the structure of SiO_2 which in fact has a lattice parameter larger than Si: this cannot happen in the case of compression. The explicit values of $\Delta_{n\text{OGB}}^{\text{nOSGB}}$ are reported for some of the structures in Table 2, while in the Supp. Mat. we reported all the values.

We observe that for the GS, contrary to the LS, there is no ambiguity in the interpretation of the sign of the pressure: an elongation (compression) of the lattice parameters implies an elongation (compression) of the bonds.

From Table 2 it's clear that oxygen segregation is strongly disadvantaged in the case of compressive strain (GS_{-0.5%}, GS_{-3.0%}), while it is favorite in the case of tensile strain for both LS and GS and with increasing number of O atoms [17,23]. Basically, the homogeneous/inhomogeneous distribution of tensile strain field around segregating sites is playing a role both in case of LS and GS, where the effect is more prominent in the case of the former than the latter. In the case of LS, we have the maximum inhomogeneous distribution of stress, whereas in case of GS the applied stress distributes homogeneously over all sites, hence its relative distortion is weak. Now as we increase the numbers of oxygen atoms, the local distortion is even more pronounced if compared to isolated

impurity and hence serving effectively on the process of segregation.

In Fig. 4 we plotted the DOS of the strained structures to analyse how the electronic properties change with respect to the pure unstrained GB and unstrained LE structures. We observe that the electronic properties are almost unchanged despite the fact that important segregation energies have been calculated in some of the strained GBs. This can be explained by the fact that silicon atoms in all the structures continue to keep their tetrahedral coordination. Only the GS induces some changes in the structure, which however seem to remain quite small.

3.2. Oxygen atoms in $\Sigma 3\{111\}$ Si GB with a Si vacancy

Oxygen atoms can also segregate in Si GBs in the presence of Si vacancies. In fact, when a vacancy is created in the GB, it induces coordination defects in the structure, which means that Si is not four-fold coordinated anymore. Therefore, Si vacancies create dangling bonds which modify both the energetic and the electronic properties of the system.

Within $\Sigma 3\{111\}$ Si GB only two distinct positions of Si exist, where vacancies can be created. These vacancies are shown in

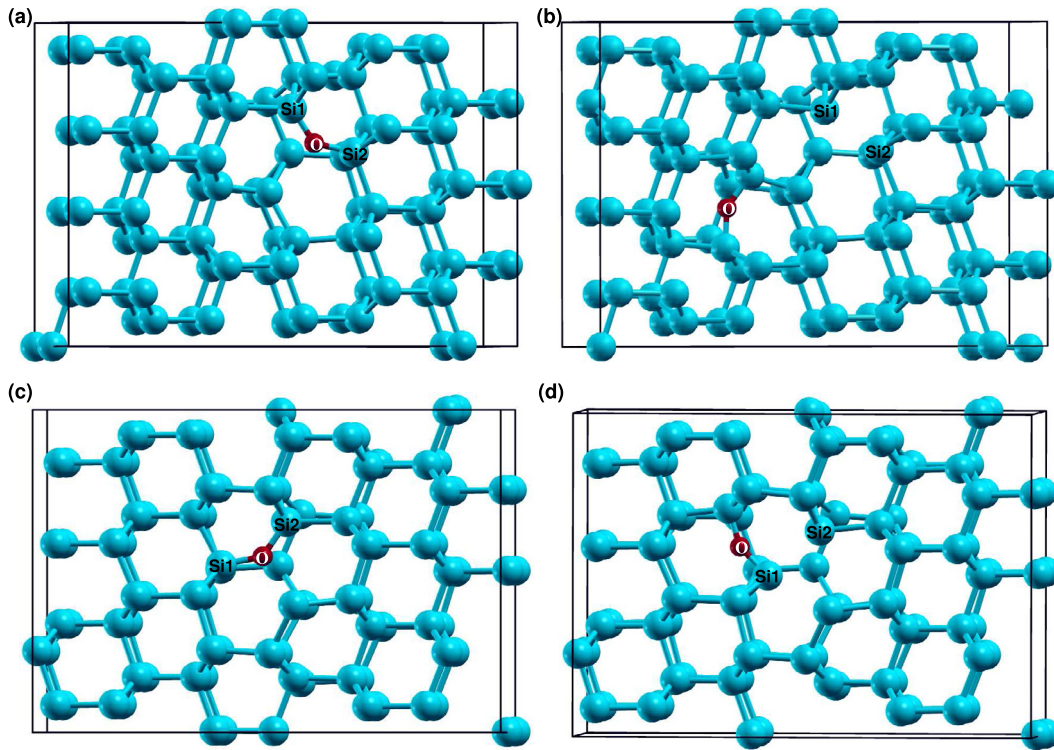


Fig. 10. $\Sigma 3\{111\}$ Si GB with V1 ((a) and (b)) or V2 ((c) and (d)) vacancy and one O atom (red ball). In (a) and (c) the O atom creates bonds with the three-fold coordinated Si atoms (Si1 and Si2) restoring the four coordination for all the atoms. In (b) and (d), the O atom places at bond-centered position between two four-fold coordinated Si atoms. The atoms Si1 and Si2 are still three-fold coordinated.

Table 3

Oxygen segregation energy Δ_{nOGB}^{nOVGB} (eV) and P_B^{nO+VGB} (GPa) for n equal to 1,2,3 and 4 oxygen atoms. The values are reported for the LE (lowest total energy) and HE (highest total energy) for V1 and V2 vacancies.

	P_B^{1O+VGB}	Δ_{1OGB}^{1OVGB}	P_B^{2O+VGB}	Δ_{2OGB}^{2OVGB}	P_B^{3O+VGB}	Δ_{3OGB}^{3OVGB}	P_B^{4O+VGB}	Δ_{4OGB}^{4OVGB}
HE _{V1}	-0.062	0.075	0.073	-0.091	0.359	0.766	0.462	-0.985
LE _{V1}	-0.276	-1.933	0.352	-2.671	1.008	-2.839	1.198	-3.073
HE _{V2}	-0.151	0.080	0.138	-0.179	0.325	-0.865	0.638	-1.076
LE _{V2}	-0.281	-1.908	0.309	-2.634	0.643	-2.824	0.876	-3.408

Fig. 9 and indicated throughout the paper as V1 and V2. The effect of creating a vacancy is that, after structural relaxation, two Si atoms become three-fold coordinated. These atoms are labelled as Si1 and Si2.

The formation energy of the vacancy in the GB is calculated as

$$E_{VGB}^f = E_{VGB} - \frac{n_{GB} - 1}{n_{GB}} E_{GB}, \quad (7)$$

where E_{VGB} is the total energy of the GB with a vacancy, n_{GB} and E_{GB} are defined in Eq. (1).[17] For V1 vacancy we found $E_{VGB}^f = 2.91$ eV, while for V2 vacancy we found $E_{VGB}^f = 3.04$ eV.

In Fig. 9 the DOS of V1 and V2 is also shown. Both V1 and V2 present a sharp peak at the bottom of the conduction which by the analysis of the projected-DOS (see inset) is due to the three-fold coordinated atoms Si1 and Si2. Another peak is also observed at around -0.5 eV in the valence band. This peak comes from the atoms Si3 and Si4 indicated on the so called V1 and V2 structures. Si3 and Si4 are four coordinated atoms but the presence of the vacancy in the GB induces strong structural distortions that are at the origin of this peak. In the pristine GB the atoms Si3 and Si4 are four-fold coordinated with angles $\sim 109.5^\circ$ and bond lengths ~ 2.35 Å, while in the presence of the vacancies the angles are $\sim 58.0^\circ$, $\sim 122.5^\circ$, $\sim 122.3^\circ$ and $\sim 115.1^\circ$ and the bond lengths change of ~ 0.2 Å.

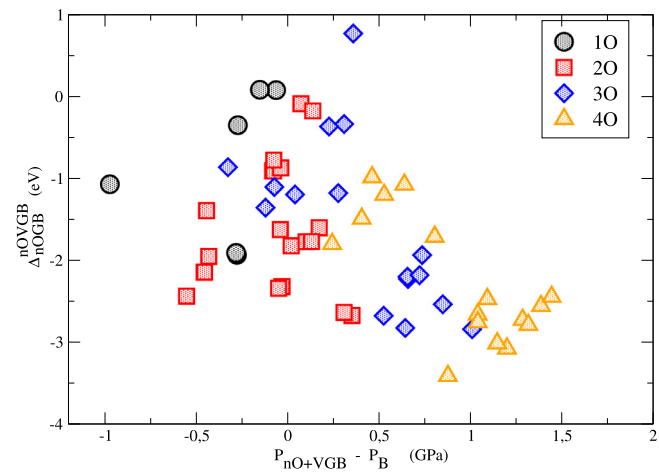


Fig. 11. O segregation energy Δ_{nOGB}^{nOVGB} as a function of P_B^{nO+VGB} . The number of O atoms is $n = 1, 2, 3$ and 4.

Starting from V1 and V2 vacancies, we inserted O atoms in different configurations and we optimised the structures. We found that two opposite situations can occur that we show in Fig. 10 for one O atom. We obtained that: 1) the O atom bonded with the

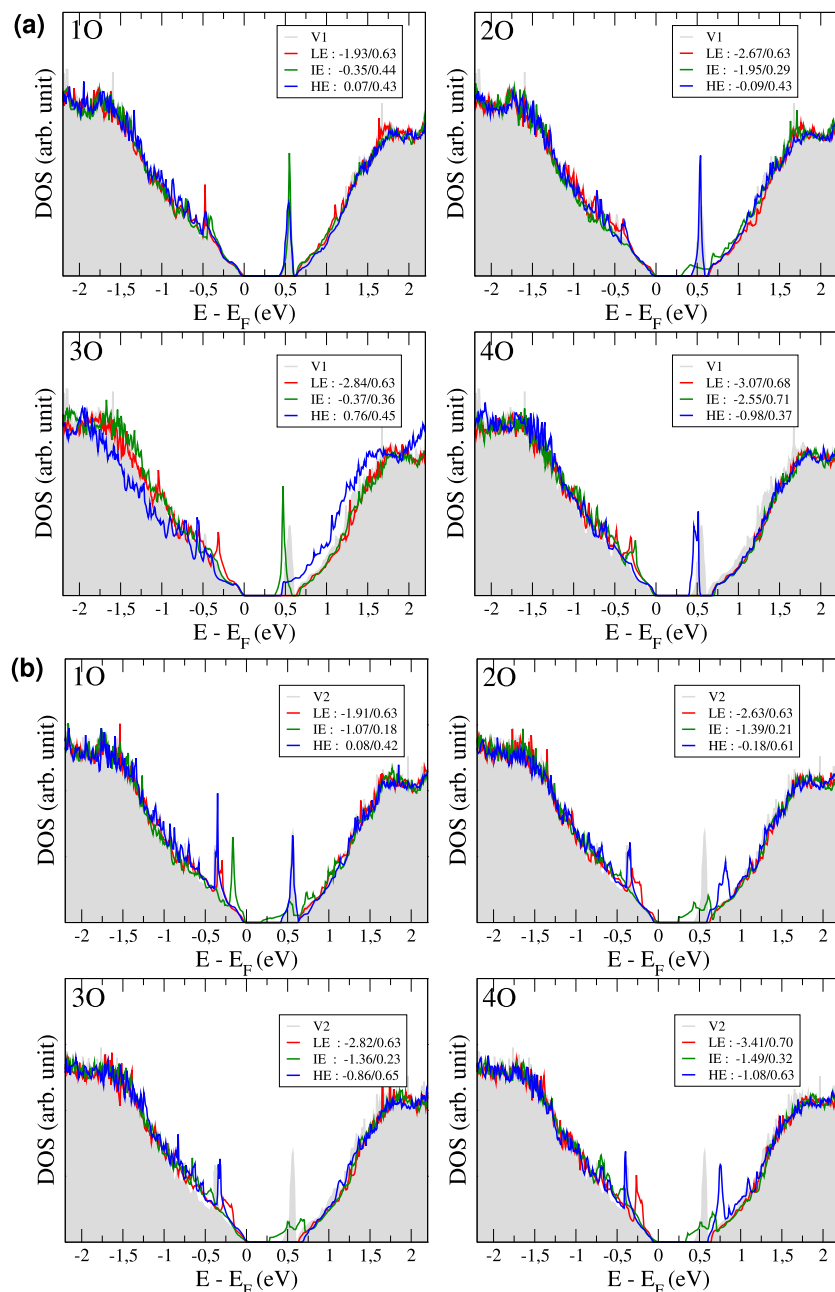


Fig. 12. The DOS of V1 (a) and V2 (b) with 1O, 2O, 3O and 4O atoms, respectively. The DOS of the GB with the vacancy only (grey shadow) is compared with that of the same structure plus an increasing number of oxygen atoms in the case of the lowest (LE red line), highest (HE blue line) and intermediate (IE green line) total energy. Numerical values in the inset are the segregation energy and the energy gap in eV, respectively.

three-fold coordinated Si1 and S2 atoms restoring the four coordination (no dangling bonds), 2) the O atom placed at bond-centered position between two four-fold coordinated Si atoms (two dangling bonds). In the case of two, three and four O atoms, we obtained the same two situations described for a single oxygen with the rest of the oxygen atoms in bond-centered positions.

The segregation energy of the O atoms at the GB with a vacancy is

$$\Delta_{n\text{OGB}}^{\text{nOVGB}} = E^{\text{nOVGB}} - E^{\text{nOGB}} \quad (8)$$

where E^{nOVGB} and E^{nOGB} are the impurity energies of the O atoms respectively in the GB with a vacancy and in the GB which are calculated as

$$E^{\text{nOVGB}} = E_{n\text{O+VGB}} - E_{\text{VGB}} - n\mu_0, \quad (9)$$

where $E_{n\text{O+VGB}}$ is the energy of the GB with a vacancy with n atoms of O, E_{VGB} is the energy of the GB with a vacancy (VGB), μ_0 is the chemical potential of the O atom, and E^{nOGB} is defined in Eq. 3 (Section 3.1).

In Fig. 11 we show the O segregation energies $\Delta_{n\text{OGB}}^{\text{nOVGB}}$ for the investigated structures as a function of their pressure $P_B^{\text{nOVGB}} = P_{n\text{O+VGB}} - P_B$ calculated as the difference between the pressure of the GB with the vacancy containing n number of O atoms ($P_{n\text{O+VGB}}$) and the pressure of the Si bulk (P_B). The explicit values of $\Delta_{n\text{OGB}}^{\text{nOVGB}}$ are reported in Table 3 for the structures with the highest and lowest segregation energy. The values for all the structures are reported in the Supp. Mat.. Similarly to strained structures, the segregation energy progressively decreases including one, two, three and four O atoms.

In Fig. 12 we plotted the DOS of V1 with 1O, 2O, 3O and 4O (top panels) and the DOS of V2 with 1O, 2O, 3O and 4O (bottom panels). We selected three configurations: the structures with the lowest total energy (LE), with the highest total energy (HE) and with intermediate total energy (IE) between LE and HE.

The behaviour of the DOS can be interpreted as following. All the LE structures have the dangling bonds saturated by an O atom (no dangling bonds). The peak at the bottom of the conduction band is therefore not present anymore. Instead, the peak in the valence band due to geometrical distortion of four-fold Si atoms in the presence of the vacancy is still present. These types of structures are the most energetically stable and have the electronic gap similar to the GB electronic gap.

The IE and HE structures have a more complex and different geometrical rearrangement of the Si and the O atoms. At the bottom of the conduction band we can find or not the peak already present in the pure V1 and V2 structures. The existence of this peak is always related to the fact that the O can saturate or not the dangling bonds of the Si atoms. Moreover, the peak, if present, can be sharp or broad. This is due to modification of the geometric structure such as bond lengths and angles with respect to their pristine counterpart (the GB with the vacancy only). The peak in the valence band instead is always due to the four-fold silicon atoms and relative structural distortions. The IE and HE structures can strongly decrease the electronic gap as many different probable segregation sites investigated have shown.

3.3. Discussion

The segregation energy mechanisms depend on local geometry distortions obtained by the GBs itself or otherwise generated by strain and/or vacancies. In $\Sigma 3\{111\}$ Si GBs, we found that O atoms do not segregate as well as other kinds of impurities such as C, B, P and Co, even if the impurity concentrations were high [16,45]. Instead, less symmetric boundaries such as $\Sigma 9\{221\}$ and $\Sigma 27\{552\}$ demonstrated to be efficient gettering centers for atomic impurities [14,26,45,47,48]. It is therefore clear that segregation is expected when the system is locally distorted.

The strain is present in GBs and induces additional local distortions. For oxygen atoms, experimental studies predict O atoms to segregate under tensile stress to attain more stable bonding network by reducing the local stress favourably in higher order grain boundary [23,45]. Through our calculations, we confirm that for O, tensile strain is always favorite and that local strain seems to be more effective than global strain. The role of strain was also pointed out for other atomic impurities such as C, B, Al, Ge, Fe and P. [15,17,19,47,49]. However, it was found that for some impurities it is the compressive strain that favours segregation.

The presence of vacancies also induces local geometrical deformation of the GB [13,19,50–52]. The segregation is favorite for those structures which have restored tetrahedral covalent bonds. The impurities become substitutional defects [15]. The presence of vacancies attract atomic impurities in order to restore the electronic stability. The same behaviour was also observed in Ni GBs with Si as impurities [53].

The electronic properties of the $\Sigma 3\{111\}$ Si GB are not significantly changed for interstitial oxygen atoms and in the presence of strain. The DOS has the same shape as for the pure GB. The oxygen atoms segregate at bond-centered position between two silicon atoms, restoring the configuration of SiO_2 . The electronic properties are therefore determined by the $\Sigma 3\{111\}$ Si GB.

Instead, a very different situation occurred in the presence of vacancies. A vacancy creates dangling bonds which can interact with the oxygen atoms segregating at the GB. The way vacancies interact with atomic impurities can be variegated and strongly depends on the number of segregated species. Predicting and then

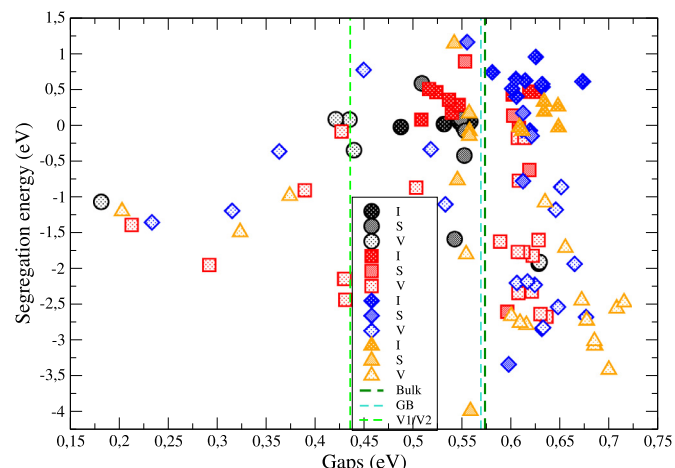


Fig. 13. The segregation energies for the $\Sigma 3\{111\}$ Si GB in presence of interstitial impurities (I, solid symbols), strain (S, heavy shading) and vacancies (V, light shading) as a function of the relative electronic band gaps. As a reference we plotted with dashed lines the Si bulk (dark green), the $\Sigma 3\{111\}$ Si GB (cyan) and the V1 and V2 (light green) electronic band gaps. Structures with increasing number of oxygen atoms are represented with different colours and symbols: 10 black circles, 20 red squares, 30 blue diamonds, 40 orange triangles.

tuning the electronic behaviour is very complicated. In fact, there exist cases where oxygen atoms can passivate dangling bonds coming from vacancies, suppressing electron-hole recombination and cases where instead deep energy states still exist.

In Fig. 13 we show the segregation energies for the $\Sigma 3\{111\}$ Si GB in presence of interstitial impurities, strain and vacancies as a function of the electronic band gaps. As a reference we also plotted the Si bulk, the $\Sigma 3\{111\}$ Si GB and the V1 and V2 electronic band gaps (V1 and V2 gaps are almost the same). The gaps of strained structures or with the presence of interstitial impurities change very little with respect to Si bulk and $\Sigma 3\{111\}$ Si GB (approximatively of about ± 0.05 eV). The behaviour is very different in the case of vacancies: actually the energy gaps of pure V1 and V2 structures is significantly smaller than that of bulk Si or GB. Moreover the presence of interstitial impurities coupled with the vacancy spreads the energy gaps in a wide range of about ± 0.3 eV around the reference value. In terms of segregation energies it can be observed that while oxygen impurities are not able to segregate in pristine $\Sigma 3\{111\}$ Si GB the presence of strain can, in some cases, favours the segregation while oxygen is always able to segregate in the presence of a Si vacancy.

4. Conclusions

We studied from first-principles the role of strain and vacancies in the segregation energy of O atoms at $\Sigma 3\{111\}$ Si GB. We considered tensile and compressive strain locally and globally applied to the GB. Then, multiple oxygen atoms were introduced in the strained GBs in many different possible configurations. For each configuration and type of strain, we calculated the oxygen segregation energy revealing the factors influencing the segregation itself. We found that oxygen segregation is always favoured by tensile strain and that local strain seems to be more effective for segregation than global one. The same methodology was then implemented to investigate the oxygen segregation in $\Sigma 3\{111\}$ Si GB with a Si vacancy: we included multiple oxygen atoms in different structural configurations, trying to deduce the mechanisms that regulate the process. The segregation is favorite for those structures which have restored a full tetrahedral coordination. The interstitial oxygen atoms, attracted by the presence of vacancies, become substitutional defects that tend to restore the electronic sta-

bility. The inhomogeneous distribution of strain field around segregating sites, due to both local geometrical distortion or the presence of a Si vacancy, is the main factor that influences the oxygen segregation at GBs.

Then we studied how the electronic properties of GBs can change due to O segregation. The correlation between strain and vacancies and the electronic structure of the GBs was pointed out. For each structure we have analysed the DOS and the band gaps versus the segregation energy as well as the projected DOS in order to characterise the origin of new energy levels. Actually, the knowledge of the nature of particular electronic states enables researchers to design new materials and strategies to reduce non radiative electron-hole recombination avoiding charge and energy losses and therefore improving solar cell efficiency.

A full understanding of the role of GBs and impurities in the solar cells performance is a very difficult problem for which further theoretical and experimental investigations would be required. The role of different types of GBs (atoms/size/order) and impurities on the electronic properties will be a future step in order to calculate and optimize the optical absorption of devices.

Declaration of Competing Interest

The authors declare that they have no known competing financial interests or personal relationships that could have appeared to influence the work reported in this paper.

Acknowledgements

We would like to thank the [University of Modena and Reggio Emilia](#) for the financial support (FAR 2018), as well as the CINECA HPC facility for the approved ISCRA C project ESGB-Si (IsC79-ESGB-Si).

Supplementary material

Supplementary material associated with this article can be found, in the online version, at doi:[10.1016/j.actamat.2020.11.019](https://doi.org/10.1016/j.actamat.2020.11.019).

References

- [1] M.A. Green, The path to 25% silicon solar cell efficiency: History of silicon cell evolution, *Prog. Photovolt: Res. Appl.* 17 (3) (2009) 183–189, doi:[10.1002/pip.892](https://doi.org/10.1002/pip.892).
- [2] A.F.B. Braga, S. Moreira, P. Zampieri, J. Bacchin, P. Mei, New processes for the production of solar-grade polycrystalline silicon: A review, *Solar Energy Materials and Solar Cells* 92 (4) (2008) 418–424, doi:[10.1016/j.solmat.2007.10.003](https://doi.org/10.1016/j.solmat.2007.10.003).
- [3] A.V. Shah, H. Schade, M. Vanecik, J. Meier, E. Vallat-Sauvain, N. Wyrsch, U. Kroll, C. Droz, J. Bailat, Thin-film silicon solar cell technology, *Progress in Photovoltaics: Research and Applications* 12 (2–3) (2004) 113–142, doi:[10.1002/pip.533](https://doi.org/10.1002/pip.533).
- [4] C.W. Lan, Growth of Multicrystalline Silicon for Solar Cells: The High-Performance Casting Method, Springer Berlin Heidelberg, Berlin, Heidelberg, pp. 175–191.
- [5] M. Imaizumi, T. Ito, M. Yamaguchi, K. Kaneko, Effect of grain size and dislocation density on the performance of thin film polycrystalline silicon solar cells, *Journal of Applied Physics* 81 (11) (1997) 7635–7640, doi:[10.1063/1.1365341](https://doi.org/10.1063/1.1365341).
- [6] H.S. Banerjee, Grain boundary effects in polycrystalline silicon solar cells, *Solar Cells* 28 (1990) 77–94, doi:[10.1016/0379-6787\(90\)90040-C](https://doi.org/10.1016/0379-6787(90)90040-C).
- [7] A. Abass, D.V. Gestel, K.V. Wiechelen, B. Maes, M. Burgelman, On the diffusion length and grain size homogeneity requirements for efficient thin-film polycrystalline silicon solar cells, *Journal of Physics D: Applied Physics* 46 (4) (2012) 045105, doi:[10.1088/0022-3727/46/4/045105](https://doi.org/10.1088/0022-3727/46/4/045105).
- [8] Y. Ohshita, Y. Nishikawa, M. Tachibana, V. Tuong, T. Sasaki, N. Kojima, S. Tanaka, M. Yamaguchi, Effects of defects and impurities on minority carrier lifetime in cast-grown polycrystalline silicon, *Journal of Crystal Growth* 275 (1) (2005) e491–e494, doi:[10.1016/j.jcrysgro.2004.11.111](https://doi.org/10.1016/j.jcrysgro.2004.11.111). Proceedings of the 14th International Conference on Crystal Growth and the 12th International Conference on Vapor Growth and Epitaxy
- [9] A. Stoffers, B. Ziebarth, J. Barthel, O. Cojocaru-Mirédin, C. Elsässer, D. Raabe, Complex nanotwin substructure of an asymmetric $\Sigma 9$ tilt grain boundary in a silicon polycrystal, *Phys. Rev. Lett.* 115 (2015) 235502, doi:[10.1103/PhysRevLett.115.235502](https://doi.org/10.1103/PhysRevLett.115.235502).
- [10] S. Wang, W.-H. Fang, R. Long, Hydrogen passivated silicon grain boundaries greatly reduce charge recombination for improved silicon/perovskite tandem solar cell performance: Time domain ab initio analysis, *The Journal of Physical Chemistry Letters* 10 (10) (2019) 2445–2452, doi:[10.1021/acs.jpcllett.9b00874](https://doi.org/10.1021/acs.jpcllett.9b00874).
- [11] J.W. Tringe, J.D. Plummer, Electrical and structural properties of polycrystalline silicon, *Journal of Applied Physics* 87 (11) (2000) 7913–7926, doi:[10.1063/1.373475](https://doi.org/10.1063/1.373475).
- [12] R. Raghunathan, E. Johlin, J.C. Grossman, Grain boundary engineering for improved thin silicon photovoltaics, *Nano Letters* 14 (9) (2014) 4943–4950, doi:[10.1021/nl501020q](https://doi.org/10.1021/nl501020q).
- [13] C.B. Feng, J.L. Nie, X.T. Zu, M.M. Al-Jassim, Y. Yan, Structure and effects of vacancies in $\Sigma 3\langle 112 \rangle$ grain boundaries in Si, *Journal of Applied Physics* 106 (11) (2009) 113506, doi:[10.1063/1.3266018](https://doi.org/10.1063/1.3266018).
- [14] D. Zhao, Y. Li, Lattice distortion induced site dependent carbon gettering at twin boundaries in silicon, *Journal of Alloys and Compounds* 712 (2017) 599–604, doi:[10.1016/j.jallcom.2017.04.111](https://doi.org/10.1016/j.jallcom.2017.04.111).
- [15] B. Ziebarth, M. Mrovec, C. Elsässer, P. Gumbsch, Interstitial iron impurities at grain boundaries in silicon: A first-principles study, *Phys. Rev. B* 91 (2015) 035309, doi:[10.1103/PhysRevB.91.035309](https://doi.org/10.1103/PhysRevB.91.035309).
- [16] Y. Ohno, K. Inoue, Y. Tokumoto, K. Kutsukake, I. Yonenaga, N. Ebisawa, H. Takamizawa, Y. Shimizu, K. Inoue, Y. Nagai, H. Yoshida, S. Takeda, Three-dimensional evaluation of gettering ability of $\Sigma 3\langle 111 \rangle$ grain boundaries in silicon by atom probe tomography combined with transmission electron microscopy, *Applied Physics Letters* 103 (10) (2013) 102102, doi:[10.1063/1.4820140](https://doi.org/10.1063/1.4820140).
- [17] P. Käshammer, T. Sinno, Interactions of twin boundaries with intrinsic point defects and carbon in silicon, *Journal of Applied Physics* 114 (8) (2013) 083505, doi:[10.1063/1.4819172](https://doi.org/10.1063/1.4819172).
- [18] A. Stoffers, O. Cojocaru-Mirédin, W. Seifert, S. Zaeferer, S. Riepe, D. Raabe, Grain boundary segregation in multicrystalline silicon: Correlative characterization by ebsd, ebic, and atom probe tomography, *Progress in Photovoltaics: Research and Applications* 23 (12) (2015) 1742–1753, doi:[10.1002/pip.2614](https://doi.org/10.1002/pip.2614).
- [19] V.Y. Lazebnykh, A.S. Mysovsky, Ab initio and atomistic simulation of local structure and defect segregation on the tilt grain boundaries in silicon, *Journal of Applied Physics* 118 (13) (2015) 135704, doi:[10.1063/1.4932203](https://doi.org/10.1063/1.4932203).
- [20] A.R. Peaker, V.P. Markevich, B. Hamilton, G. Parada, A. Dudas, A. Pap, E. Don, B. Lim, J. Schmidt, L. Yu, Y. Yoon, G. Rozgonyi, Recombination via point defects and their complexes in solar silicon, *physica status solidi (a)* 209 (10) (2012) 1884–1893, doi:[10.1002/pssa.201200216](https://doi.org/10.1002/pssa.201200216).
- [21] L. Chen, X. Yu, P. Chen, P. Wang, X. Gu, J. Lu, D. Yang, Effect of oxygen precipitation on the performance of czochralski silicon solar cells, *Solar Energy Materials and Solar Cells* 95 (11) (2011) 3148–3151, doi:[10.1016/j.solmat.2011.06.044](https://doi.org/10.1016/j.solmat.2011.06.044).
- [22] Y. Ohno, K. Inoue, K. Fujiwara, M. Deura, K. Kutsukake, I. Yonenaga, Y. Shimizu, K. Inoue, N. Ebisawa, Y. Nagai, Three-dimensional evaluation of gettering ability for oxygen atoms at small-angle tilt boundaries in czochralski-grown silicon crystals, *Applied Physics Letters* 106 (25) (2015) 251603, doi:[10.1063/1.4921742](https://doi.org/10.1063/1.4921742).
- [23] Y. Ohno, K. Inoue, K. Fujiwara, K. Kutsukake, M. Deura, I. Yonenaga, N. Ebisawa, Y. Shimizu, K. Inoue, Y. Nagai, H. Yoshida, S. Takeda, S. Tanaka, M. Kohyama, Impact of local atomic stress on oxygen segregation at tilt boundaries in silicon, *Applied Physics Letters* 110 (6) (2017) 062105, doi:[10.1063/1.4975814](https://doi.org/10.1063/1.4975814).
- [24] C.H. Seager, Grain boundaries in polycrystalline silicon, *Annual Review of Materials Science* 15 (1) (1985) 271–302, doi:[10.1146/annurev.ms.15.080185.001415](https://doi.org/10.1146/annurev.ms.15.080185.001415).
- [25] T.T. Shi, Y.H. Li, Z.Q. Ma, G.H. Qu, F. Hong, F. Xu, Y. Yan, S.-H. Wei, First-principles study of iron segregation into silicon $\Sigma 5$ grain boundary, *Journal of Applied Physics* 107 (9) (2010) 093713, doi:[10.1063/1.3369390](https://doi.org/10.1063/1.3369390).
- [26] C.H. Liebscher, A. Stoffers, M. Alam, L. Lymparakis, O. Cojocaru-Mirédin, B. Gault, J. Neugebauer, G. Dehm, C. Scheu, D. Raabe, Strain-induced asymmetric line segregation at faceted si grain boundaries, *Phys. Rev. Lett.* 121 (2018) 015702, doi:[10.1103/PhysRevLett.121.015702](https://doi.org/10.1103/PhysRevLett.121.015702).
- [27] J. Lu, M. Wagener, G. Rozgonyi, J. Rand, R. Jonczyk, Effects of grain boundary on impurity gettering and oxygen precipitation in polycrystalline sheet silicon, *Journal of Applied Physics* 94 (1) (2003) 140–144, doi:[10.1063/1.1578699](https://doi.org/10.1063/1.1578699).
- [28] S. Pizzini, P. Cagnoni, A. Sandrinelli, M. Anderle, R. Canteri, Grain boundary segregation of oxygen and carbon in polycrystalline silicon, *Applied Physics Letters* 51 (9) (1987) 676–678, doi:[10.1063/1.98331](https://doi.org/10.1063/1.98331).
- [29] J. Chen, T. Sekiguchi, Carrier recombination activity and structural properties of small-angle grain boundaries in multicrystalline silicon, *Japanese Journal of Applied Physics* 46 (10A) (2007) 6489–6497, doi:[10.1143/jjap.46.6489](https://doi.org/10.1143/jjap.46.6489).
- [30] Y. Ohno, K. Inoue, K. Fujiwara, K. Kutsukake, M. Deura, I. Yonenaga, N. Ebisawa, Y. Shimizu, K. Inoue, Y. Nagai, H. Yoshida, S. Takeda, S. Tanaka, M. Kohyama, Nanoscopic analysis of oxygen segregation at tilt boundaries in silicon ingots using atom probe tomography combined with tem and ab initio calculations, *Journal of Microscopy* 268 (3) (2017) 230–238, doi:[10.1111/jmi.12602](https://doi.org/10.1111/jmi.12602).
- [31] G. Sarau, S. Christiansen, M. Holla, W. Seifert, Correlating internal stresses, electrical activity and defect structure on the micrometer scale in EFG silicon ribbons, *Solar Energy Materials and Solar Cells* 95 (8) (2011) 2264–2271, doi:[10.1016/j.solmat.2011.03.039](https://doi.org/10.1016/j.solmat.2011.03.039).
- [32] H. Ogawa, Gbstudio: A builder software on periodic models of csl boundaries for molecular simulation, *Materials Transactions* 47 (11) (2006) 2706–2710, doi:[10.2320/matertrans.47.2706](https://doi.org/10.2320/matertrans.47.2706).
- [33] O.H. Nielsen, R.M. Martin, Stresses in semiconductors: Ab initio calculations on Si, Ge, and GaAs, *Phys. Rev. B* 32 (1985) 3792–3805, doi:[10.1103/PhysRevB.32.3792](https://doi.org/10.1103/PhysRevB.32.3792).

- [34] G. Kresse, J. Hafner, Ab initio molecular dynamics for liquid metals, *Phys. Rev. B* 47 (1993) 558.
- [35] G. Kresse, J. Furthmüller, Efficient iterative schemes for ab initio total-energy calculations using plane-wave basis set, *Phys. Rev. B* 54 (1996) 11169.
- [36] J.P. Perdew, K. Burke, M. Ernzerhof, Generalized gradient approximation made simple, *Phys. Rev. Lett.* 77 (1996) 3865–3868, doi:10.1103/PhysRevLett.77.3865.
- [37] H.J. Monkhorst, J.D. Pack, Special points for brillouin-zone integrations, *Physical Review B* 13 (12) (1976) 5188.
- [38] P.E. Blöchl, O. Jepsen, O.K. Andersen, Improved tetrahedron method for brillouin-zone integrations, *Phys. Rev. B* 49 (1994) 16223–16233, doi:10.1103/PhysRevB.49.16223.
- [39] P. Haas, F. Tran, P. Blaha, K. Schwarz, R. Laskowski, Insight into the performance of GGA functionals for solid-state calculations, *Phys. Rev. B* 80 (2009) 195109, doi:10.1103/PhysRevB.80.195109.
- [40] G.I. Csonka, J.P. Perdew, A. Ruzsinszky, P.H.T. Philipsen, S. Lebègue, J. Paier, O.A. Vydrov, J.G. Ángyán, Assessing the performance of recent density functionals for bulk solids, *Phys. Rev. B* 79 (2009) 155107, doi:10.1103/PhysRevB.79.155107.
- [41] E. Luppi, H.-C. Weissker, S. Bottaro, F. Sottile, V. Vénard, L. Reining, G. Onida, Accuracy of the pseudopotential approximation in ab initio theoretical spectroscopies, *Phys. Rev. B* 78 (24) (2008) 245124.
- [42] S. Refaelly-Abramson, M. Jain, S. Sharifzadeh, J.B. Neaton, L. Kronik, Solid-state optical absorption from optimally tuned time-dependent range-separated hybrid density functional theory, *Phys. Rev. B* 92 (2015) 081204, doi:10.1103/PhysRevB.92.081204.
- [43] N. Gauriot, V. Vénard, E. Luppi, Long-range corrected exchange-correlation kernels to describe excitons in second-harmonic generation, *The Journal of Chemical Physics* 151 (23) (2019) 234111, doi:10.1063/1.5126501.
- [44] A.J. Morris, C.J. Pickard, R.J. Needs, Hydrogen/nitrogen/oxygen defect complexes in silicon from computational searches, *Phys. Rev. B* 80 (2009) 144112, doi:10.1103/PhysRevB.80.144112.
- [45] Y. Ohno, K. Kutsukake, M. Deura, I. Yonenaga, Y. Shimizu, N. Ebisawa, K. Inoue, Y. Nagai, H. Yoshida, S. Takeda, Recombination activity of nickel, copper, and oxygen atoms segregating at grain boundaries in mono-like silicon crystals, *Applied Physics Letters* 109 (14) (2016) 142105, doi:10.1063/1.4964440.
- [46] E. Luppi, E. Degoli, M. Bertocchi, S. Ossicini, V. Vénard, Strain-designed strategy to induce and enhance second-harmonic generation in centrosymmetric and noncentrosymmetric materials, *Phys. Rev. B* 92 (2015) 075204, doi:10.1103/PhysRevB.92.075204.
- [47] D. Zhao, Y. Li, Revealing the factors influencing grain boundary segregation of p, as in si: Insights from first-principles, *Acta Materialia* 168 (2019) 52–62, doi:10.1016/j.actamat.2019.02.014.
- [48] A. Maiti, M.F. Chisholm, S.J. Pennycook, S.T. Pantelides, Dopant segregation at semiconductor grain boundaries through cooperative chemical rebonding, *Phys. Rev. Lett.* 77 (1996) 1306–1309, doi:10.1103/PhysRevLett.77.1306.
- [49] P. Käshammer, T. Sinnö, A mechanistic study of impurity segregation at silicon grain boundaries, *Journal of Applied Physics* 118 (9) (2015) 095301, doi:10.1063/1.4929637.
- [50] P.B. Allen, W.E. Pickett, H. Krakauer, Anisotropic normal-state transport properties predicted and analyzed for high- T_c oxide superconductors, *Phys. Rev. B* 37 (1988) 7482–7490, doi:10.1103/PhysRevB.37.7482.
- [51] M.J. Puska, S. Pöykkö, M. Pesola, R.M. Nieminen, Convergence of supercell calculations for point defects in semiconductors: Vacancy in silicon, *Phys. Rev. B* 58 (1998) 1318–1325, doi:10.1103/PhysRevB.58.1318.
- [52] X. Zhang, Y. Duan, X. Dai, T. Li, Y. Xia, P. Zheng, H. Li, Y. Jiang, Atomistic origin of amorphous-structure-promoted oxidation of silicon, *Applied Surface Science* 504 (2020) 144437, doi:10.1016/j.apsusc.2019.144437.
- [53] M. Mazalová, M. Všianská, J. Pavlù, M. Šob, The effect of vacancies on grain boundary segregation in ferromagnetic fcc Ni, *Nanomaterials* (Basel, Switzerland) 10 (4) (2020) 691, doi:10.3390/nano10040691. 32268587[pmid]